molecular pharmaceutics

Article

pubs.acs.org/molecularpharmaceutics

Permeability Profiles and Intestinal Toxicity Assessment of Hydrochlorothiazide and Its Inclusion Complex with β-Cyclodextrin Loaded into Chitosan Nanoparticles

R. Onnainty,[†] E. M. Schenfeld,[†] J. P. Petiti,[‡] M. R. Longhi,[†] A. Torres,[‡] M. A. Quevedo,[†] and G. E. Granero*[,†]

[†]Departamento de Farmacia, UNITEFA, CONICET, Facultad de Ciencias Químicas, Universidad Nacional de Córdoba, Córdoba, X5000HUA, Argentina

[‡]Centro de Microscopía Electrónica, UNC, INICSA, CONICET, Facultad de Ciencias Químicas, Universidad Nacional de Córdoba, Córdoba, X5000HUA, Argentina

ABSTRACT: Here, a novel drug delivery system was developed for the hydrochlorothiazide (HCT):β-cyclodextrin (βCD) inclusion complex loaded into chitosan (CS) nanoparticles (NPs) [CS/HCT:βCD NPs]. It was found, for the first time, that exposure of the intestinal mucosa to free HCT resulted in an increased and abnormal intestinal permeability associated with several injuries to the intestinal epithelium. Nevertheless, the HCT delivery system obtained ameliorated the damage of the intestinal epithelium induced by HCT. Furthermore, we found that the corresponding permeability profiles for both the free HCT and the CS/HCT:βCD NPs were exponential and lineal, respectively. We propose that the increased intestinal uptake and severe tissue injury of HCT to the intestinal epithelium could be directly related to possible effects of this drug on the ionoregulatory Na^{+}/K^{+}-ATPase channel. Thus, it is postulated that the CS/HCT:βCD NPs may increase the gastrointestinal retention of the HCT, which would provide increased adherence to the mucus barrier that lines the intestinal epithelium; consequently, this would act as a slow HCT release delivery system and maintain lower drug levels of luminal gut in comparison with the administration of free HCT, leading to less severe local injury.

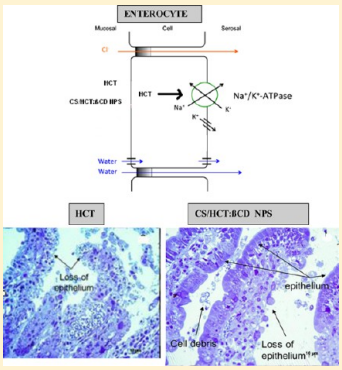

KEYWORDS: *hydrochlorothiazide, inclusion complex, chitosan nanoparticles, mucoadhesion, absorption profiles, toxicity*

1. INTRODUCTION

Hydrochlorothiazide (HCT, 6-chloro-3,4-dihydro-2*H*-1,2,4-benzo-thiodiazine-7- sulfonamide-1,1-dioxide) is commonly prescribed as an antihypertensive drug.[1] HCT presents a low bioavailability but with a large variation in this parameter, ranging from 60% to 80%, which is relatively dose proportional.[2] HCT was classified as a drug type IV under the Biopharmaceutics Classification Systems (BCS).[3] Its low and variable oral bioavailability could be due to its low solubility and therefore slow dissolution and low intestinal permeability.[4]

Drug delivery carriers offer the potential to improve some of the unfavorable biopharmaceutic drug properties, with in particular the polymeric nanoparticles (NPs) being considered a very interesting strategy to achieve this aim.[5]

NPs composed of the natural polysaccharide chitosan (CS) are particularly promising for transmucosal drug delivery applications, due to their biocompatibility and mucoadhesion features.[6]

CS is an abundant and linear natural polysaccharide[7] formed by glucosamine and *N*-acetylglycosamine units, with a pK_a value of 6.3−7 and a positive charge conferred by a primary amino group and two free hydroxyl groups.[8] CS can form nanoparticulate systems combined with suitable cross-linking agents such as polyethylene glycol (PEG), dicarboxylic acids, or tripolyphosphate (TPP).[9]

It has been reported that chitosan nanoparticles (CS NPs) are good hydrophilic drug carriers although they are not sufficiently good enough for delivering lipophilic drugs. The combination of CS with cyclodextrins (CDs) was proposed as a strategy to encapsulate both hydrophilic and lipophilic drugs. These CS/CD NPs might improve the bioavailability of hydrophobic drugs such as HCT by enhancing their solubility and permeability features.[10]

CDs may include fully or partially hydrophobic drugs in their hydrophobic cavity to form inclusion complexes, which behave as carriers of poorly soluble drugs due to the hydrophilic external surface. Also, the formation of inclusion complexes might increase drug stability and improve drug bioavailability.[11] Due to the low cost and appropriate size of its hydrophobic cavity, β-cyclodextrin (βCD) is often selected from the available CDs.

Received: June 14, 2016
Revised: October 14, 2016
Accepted: October 18, 2016
Published: October 18, 2016

DOI: 10.1021/acs.molpharmaceut.6b00532
Mol. Pharmaceutics XXXX, XXX, XXX−XXX

We have demonstrated that the formation of inclusion complexes between HCT and βCD significantly improves the solubility of HCT.[12] The prior formation of an inclusion complex between drugs with CDs is a strategy used to incorporate the drug into the hydrophilic polymer to obtain hydrophilic polymer/CDs NPs, which generally results in a greater loading drug capacity. This strategy combines both the solubilizing properties of CDs and the prolonged release and absorption enhancer properties of CS.[13]

The aim of this work was to study the capacity of CS/βCD NPs to improve the oral bioavailability of HCT. For this purpose, we chose to combine CS with βCD, which is a solubility enhancer of the hydrophobic drug HCT, in order to achieve the maximum concentration of HCT into CS NPs. Thus, here CS/HCT:βCD NPs were obtained via the cross-linking method to deliver HCT of which CS NPs with different CS/TPP molar ratios were obtained in order to select the one with the most advantageous characteristics for oral drug delivery. Subsequently, CS NPs were characterized considering their size, encapsulation efficiency, and *in vitro* drug release properties, at different pH values, to assess their performance in releasing the HCT. The mucoadhesion mechanism was explored in relation to mucin adsorption, while the permeation behavior through the rat intestinal wall was evaluated with respect to *ex vivo* transport in rat intestine using everted rat intestinal sacs. Finally, the effect of the NPs on the intestinal mucosa of rats was also assessed.

2. EXPERIMENTAL METHODS

2.1. Materials. HCT was bought from Parafarm (Buenos Aires, Argentina) and used without further purification. βCD was generously donated by Ferromet S.A. (agent of Roquette in Argentina). Low molecular weight chitosan (CS, 85% deacetylation degree) was obtained from Sigma-Aldrich (Buenos Aires, Argentina), and pentasodium tripolyphosphate (TPP) was acquired from Todo Droga (Córdoba, Argentina). Mucin from porcine stomach type II and tissue culture medium TC 199 were purchased from Sigma-Aldrich (Buenos Aires, Argentina). The enzymatic glucose kit was obtained from the Wiener lab (Rosario, Argentina), and the water used in these studies was generated with a Milli-Q Water Purification System (Millipore Bedford, USA). Chemicals were of reagent grade or higher.

2.2. Preparation of Nanoparticles. *2.2.1. Preparation of Blank CS NPs.* The CS NPs were obtained by ionic gelation, according to a method proposed by Fan et al.,[14] with slight modifications. Briefly, several concentrations (0.25, 0.5, 0.75, and 1.0 mg/mL) of CS were dissolved in acetic acid (four times lower than the CS concentration). After the mixture was stirred vigorously, it was stored overnight at room temperature. Then, the pH was adjusted to 4.9 with a 1 N NaOH aqueous solution under magnetic stirring. In order to form NPs, 10 mL of a heated (at 60 °C) CS solution was mixed with 3 mL of a cooled TPP aqueous solution (4 °C, pH 5.5 and at various concentrations 0.25, 0.5, 0.75, and 1.0 mg/mL) under constant magnetic stirring at room temperature. The optimum time was determined to be 10 min. After centrifugation at 13,000 rpm for 40 min (20 °C) in the presence of 10 μL of glycerol, the NPs were washed twice with distilled water.

2.2.2. Preparation of the HCT:βCD Inclusion Complex. The HCT:βCD inclusion complex was prepared according to our previously reported method, by which a 1:1 complex was obtained and exhaustively characterized.[12] Briefly, 0.0298 g of HCT were mixed with 0.1135 g of βCD in a phosphate buffer solution (pH 7.4) under magnetic agitation. After which, the suspension was sonicated for 2 h at room temperature. Finally, the resulting suspension was filtered through a 0.45 μm membrane to remove any undissolved solid.

2.2.3. Preparation of CS NPs Loaded with the HCT:βCD Inclusion Complex. To obtain the CS NPs loaded with HCT:βCD, CS was dissolved in acetic acid at a concentration of 2 mg/mL, and in this way the positive charge improved the CS water solubility. A TPP stock solution (2 mg/mL) was added to 10 mL of HCT:βCD inclusion complex solutions previously filtered through 0.45 μm cellulose acetate membrane filters. The CS/HCT:βCD NPs were spontaneously formed upon addition of the inclusion complex/TPP mixture to the CS solution. These CS/HCT:βCD NPs were obtained by using mass ratios of CS and TPP of 3:1. The NPs suspensions were continuously stirred for 10 min and centrifuged at 13,000 rpm for 40 min at 20 °C in the presence of 10 μL of glycerol to prevent NP aggregation.

2.3. Physicochemical and Morphological Characterization of NPs. The average particle size, polydispersity index (PDI), and zeta potential (ZP) of the obtained NPs were evaluated using dynamic light scattering (DLS) (Zetasizer Delsa Nano Version 2.20, Beckman Coulter Inc.) All measurements were carried out in triplicate at 25 °C. The suspension of the NPs was appropriately diluted with milli-Q water to attain suitable concentrations for analysis. The diameter and PDI of particle sizes were estimated using the CONTIN algorithm analysis through inverse Laplace Transformation of the autocorrelation function.

The surface morphology of both empty and drug-loaded NPs was observed by scanning electron microscopy (SEM), using a SUPRA 40 (ZEISS) analytical scanning electron microscope. Energy-dispersive X-ray spectroscopy (EDX) analysis was obtained using an EDX detector connected with an FE-SEM (FE-SEM, Zeiss: Σigma series, Jena, Germany).

2.4. Evaluation of HCT Encapsulation Efficiency into CS NPs. The encapsulation efficiency (EE) of HCT into particles was determined indirectly. CS NPs were separated from unbound HCT by centrifugation (13,000 rpm, 40 min), and free HCT in the supernatant was quantified by UV−V spectrometry (λ = 270 nm). The %EE was calculated as follows (eq 1):

$$\%EE = \frac{HCT_{total} - HCT_{free}}{HCT_{total}} \quad (1)$$

2.5. Long-Term Stability of NPs in Water and Buffer Solutions. The long-term stability of CS and CS/HCT:βCD suspensions of NPs was assessed at different storage pHs (1.2, 5.5, 6.8, and 7.4) and in water. Experiments were conducted for 20 days at room temperature. Analyses were performed on days 1, 7, 14, and 20. Samples were evaluated for particle size and PDI by the DLS instrument.

2.6. *In Vitro* Drug Release Studies. The release profiles of CS/HCT:βCD, HCT, and the starting HCT:βCD inclusion complex were obtained by the dialysis method. The dialysis membrane with a MWCO of 12,000 Da formed a tube containing 5 mL of the donor solution, which in turn contained a pellet of NPs with an amount of HCT:βCD complex equivalent to 350 μg of HCT, an HCT:βCD complex equivalent to 350 μg of HCT, or 350 μg of HCT. The resulting dialysis bag was immersed in 50 mL of PBS pH 7.4

DOI: 10.1021/acs.molpharmaceut.6b00532
Mol. Pharmaceutics XXXX, XXX, XXX−XXX

release medium in order to mimic gastrointestinal conditions (corresponding to the mucus layer of small intestine and at physiological conditions), at room temperature, and under agitation. Aliquots of the release medium were sampled and replaced with equivalent fresh medium for 24 h. Experiments were performed in triplicate. The amount of HCT in the release medium was determined at 270 nm by a UV/vis spectrophotometer (Agilent Technologies Cary 60 UV−vis spectrometer).

2.7. *In Vitro* HCT Release from CS/HCT:βCD NPs in the Presence of Mucin. To establish a mechanism through which the CS/HCT:βCD NPs release the loaded drug, *in vitro* drug release assays were performed by incubating CS/HCT:βCD NPs in a phosphate buffered saline solution at pH 7.4 containing 1.0% of mucin and stirred at 37 ± 0.5 °C. All samples were withdrawn at 2 h, with this study being performed in triplicate. The sample preparation technique was performed according to a previously described technique (section 2.9.4), and measurements were recorded following the HPLC analysis protocol detailed in section 2.9.5.

2.8. Mucoadhesion Studies. *2.8.1. Mucin Particle Method.* Mucoadhesive properties of CS/HCT:βCD NPs were studied using the mucin particle method.[15] In this technique, a commercial mucin (pig gastric mucin (PGM)) is used. The ZP change of the mucin particles due to the presence of NPs was an indication of mucoadhesion. Briefly, PGM suspended in PBS (pH 7.4) at a concentration of 0.4 mg/mL was mixed with an appropriate amount of CS/HCT:βCD NPs in PBS (pH 7.4) at room temperature. After incubation for 24 h, the ZP was measured.

2.8.2. Scanning Electron Microscopy (SEM) for the Investigation of Mucin Interactions with NPs. PGM was suspended in PBS buffer (pH 7.4) at a concentration of 1 mg/L in the presence or absence of CS/HCT:βCD NPs suspended in PBS buffer (pH 7.4). Following equilibration at room temperature (24 h), aliquots of the gels obtained were dried by vacuum and sputtered with gold to be analyzed by scanning electron microscopy. Imaging was carried out using an accelerating voltage of 3 kV and the secondary electron detector on an electronic microscope (SUPRA 40 (ZEISS) scanning electron microscopy).

2.9. Intestinal Permeation Studies. *2.9.1. Animal Treatments.* The Committee of Ethics for the Use of Animals from the Faculty of Chemical Sciences, National University of Córdoba, Argentina approved the present protocol (Res. No. 138/07). Healthy male Wistar rats were used at the age of 3 months (300−350 g). Animals had free access to water and food pellets until 24 h before the experiments were performed. After that, they were fasted and allowed to ingest water *ad libitum* until surgical procedures were performed.

2.9.2. In Vitro Intestinal Permeation Study. The intestinal permeations of HCT, HCT:βCD, and CS/HCT:βCD NPs were investigated by using the intestinal gut sac technique.[16−19]

After anesthetizing the rats by an intraperitoneal administration of urethane (1000 mg/kg), an abdominal incision of 2 cm was made to isolate a segment of 10 cm of the proximal jejunum (15 cm distal to the ligament of Treitz). After this procedure, rats were sacrificed with CO_2. Intestinal segments were cleaned with 30 mL of oxygenated TC 199 (37 °C, 5% CO_2 and 95% O_2). To study the apical-to-basal (A/B) transport, segments were everted over a glass rod. Intestinal sacs were placed in an apparatus described in a previous publication, following the procedure described therein.[18] For HCT, two concentration levels (1 and 17 μg/mL) were added to the oxygenated TC 199 dissolved in 50 μL of dimethyl sulfoxide. The tissue viability was monitored by means of glucose concentration test previously reported.[19]

Intestinal permeability assays were carried out by placing 1 mL of pH 7.4 oxygenated TC 199 (5:95 CO_2/O_2, 37 °C) in the serosal side of the sacs. Then, aliquots were withdrawn at 10, 20, 30, 40, 50, 60, 70, 80, 90, 100, 110, and 120 min from the sacs and replaced by 1 mL of drug-free oxygenated TC 199. Between trials, the cannula was cleaned with 1 mL of pH 7.4 oxygenated TC 199 (37 °C), adding the washing medium to the corresponding permeation sample.

Aliquots obtained from the serosal side of sacs were processed following the procedure detailed in section 2.9.4, and then analyzed by HPLC using the protocol described in section 2.9.5. Assays were performed in triplicate at each assayed concentration and experimental setup. After 2 h transport study, the apparent permeability coefficient (P_{app} cm/min) was calculated applying eq 2:

$$P_{app} = \frac{F}{SAxC_o}$$
$$SA = 2\pi rh \quad (2)$$

where SA is the surface area of the barrier membrane (cm^2); C_o is the initial drug concentration (μg/mL) in the mucosal compartment, r is the intestinal segment mean radius (0.40 cm), and h is the length of the intestinal segment (10 cm).

Studies were performed in triplicate, and all data were expressed as means ± SD. Data were analyzed by a one-way ANOVA. A difference was considered statistically significant when $p < 0.05$.

2.9.3. Gut Sac Viability. Glucose concentrations were measured in the mucosal and serosal solutions following a method proposed by Lifschitz et al. with some changes.[16] The intestinal epithelium was considered as viable and metabolically healthy when it was able to concentrate glucose on the serosal side of sacs because glucose is transported across the intestinal mucosa by an active carrier. Tissue viability studies were conducted for 120 min, with glucose quantification being performed every 10 min. The mucosal solutions consisted of drug-free TC199 or solutions containing the corresponding concentrations of HCT or CS/HCT:βCD NPs. The glucose concentration was quantified using a commercial assay (Wiener) and applying the protocol detailed in a previous publication.[19]

2.9.4. Sample Preparation for HCT Quantification. The analyte was separated from the TC 199 medium by a developed and fully validated solid phase extraction (SPE) procedure. Strata-X (60 mg, Phenomenex) SPE cartridges were used. The following scheme of extraction was applied: (a) cartridges were preconditioned applying 2.0 mL of methanol HPLC grade ($MeOH_{HPLC}$), after which (b) an aliquot of 2.0 mL of pH 2 (100 mM) phosphate buffer was added to equilibration. The analytical sample was prepared by adding the Internal Standard (IS) solution (caffeine, 50 μL, 3.7 μg/mL) to the corresponding sampled aliquots, which were homogenized and (c) applied to the preconditioned cartridge at a flow rate of 1 drop/s. Afterward, (d) the cartridge was dried under vacuum for 1 min, and finally (e) the analyte elution was achieved by applying 1 mL of HPLC grade acetonitrile (ACN_{HPLC}). Prior to HPLC analysis, (f) the eluted sample was concentrated under a

DOI: 10.1021/acs.molpharmaceut.6b00532
Mol. Pharmaceutics XXXX, XXX, XXX−XXX

Table 1. Conditions Tested To Obtain CS and TPP NPs

	CS (mg/mL)							
	0.5		1.0		1.5		4.0	
TPP (mg/mL)	size (nm)	PDI	size (nm)	PDI	size (nm)	PDI	size (nm)	PDI
0.25	opalescent		opalescent		opalescent		clear solution	
	242.4	0.377	326.0	0.320	416.7	0.382		
0.5	opalescent		opalescent		opalescent		clear solution	
	327.6	0.264	317.2	0.294	255.2	0.208		
0.75	aggregation		aggregation		opalescent		aggregation	
					573.2	0.541		
1.0	aggregation		aggregation		aggregation		opalescent	
							665.9	0.285

N_2 stream at 40 °C and resuspended in 200 μL of a MeOH/H_2O 50:50 mixture.

2.9.5. Quantitative (HPLC) Analyses. The HPLC system used was a Jasco chromatograph, equipped with a quaternary pump and a Jasco Multiple Wavelenght detector (Jasco UV-2077 Plus) set at 270 nm. Chromatographic separations were carried out on a C18 Restek (15 cm × 4.5 mm × 5 μm) column thermostatized at 30 °C. A Phenomenex Security Guard Fusion RP (4 × 30 mm) guard column was also employed. Chromatographic analyses were performed in the gradient mode, with the mobile phase consisting of acetic acid in water (pH = 3.6): $MeOH_{HPLC}$ (80:20, v/v) for 5 min, which linearly changed to (50:50 v/v) for 4 min, after which it was kept constant for another 2 min. Finally, the solvent composition was linearly modified back to its original ratio (80:20, v/v) in 1 min to ensure column re-equilibration prior to the following injection. The total run time was 12 min. The eluent was pumped at a flow rate of 1 mL/min, with a sample injection volume of 15 μL.

2.9.6. Stability of NPs in TC 199 Cultured Medium. The stability of CS/HCT:βCD NPs in the TC 199 culture medium was studied by observation of the hydrodynamic radius change. The NPs were incubated in TC 199 culture medium at pH 7.4 for 2 h at 37 °C. The changes in the particle hydrodynamic radius and the PDI were monitored by DLS.

2.10. Toxicology Studies. The integrity of intestinal tissues was determined by histological examination of the intestinal sacs obtained after the permeability studies. Sections of intestinal sacs treated with HCT (dose of 17 μg/mL), HCT:βCD (equivalent amount of 17 μg/mL of HCT), and CS/HCT:βCD NPs were opened longitudinally along the mesenteric border, and fixed in Karnovsky's solution (4% formaldehyde and 1.5% glutaraldehyde in 0.1 M sodium cacodylate buffer pH 7.4) for 2 h at room temperature. After washing the samples with 0.1 M sodium cacodylate buffer pH 7.4 (three times), they were treated with 1% osmium tetroxide for 2 h, and stained in block with 1% uranyl acetate in 0.1 M acetate buffer, pH 5.2, for 20 min. The dehydration of samples was performed with a series of graded cold acetones. After this samples were embedded in Araldite. For light microscopy, 1 μm thick sections were cut serially and stained with a 1% toluidine blue and 1% borax solution. For ultrastructural studies, thin sections were cut with a diamond knife on a JEOL JUM-7 ultramicrotome, stained with uranyl acetate/lead citrate and examined using a Zeiss LEO 906E electron microscope.

3. RESULTS AND DISCUSSION

3.1. NPs Preparation, Characterization, and Drug Encapsulation Efficiency (EE). The NPs of CS and TPP, empty or loaded with HCT:βCD, were obtained by the ionotropic gelation method. Several parameters can be varied during the fabrication of the NPs, such as their size, ZP, and PDI.

A series of experiments were performed to select the reagent ratios to obtain the best CS:TPP NPs. Opalescence was used as the signal that NPs were formed, which then was demonstrated by means of DLS. Results are displayed in Table 1.

NPs were obtained at CS:TPP weight ratios of 2:1 and 4:1. In the presence of TPP, CS formed a gel due to inter- and intramolecular cross-linkages to the anionic TPP.[20] However, with higher amounts of TPP turbidity was observed due to the formation of aggregates. When the amount of TPP was even greater, the particles aggregated established unions with TPP molecules, which led to their flocculation (CS/TPP mass ratio lower than 2:1). Samples were analyzed taking into account the particle size and the reproducibility. The results indicated that a CS/TPP ratio of 3:1 yielded the best CS NPs, which had an average size of 220 nm and a positively charged superfice (Table 2).

Table 2. Physicochemical Characteristics of CS NPs

	size (nm)	PDI	zeta potential (mV)
CS NPs	223	0.253	49
CS/HCT:βCD NPs	390	0.191	33

In this work, CS NPs loaded with HCT:βCD were obtained following a two-step procedure. The HCT:βCD inclusion complex was obtained in a first stage, after which the inclusion complex HCT:βCD was entrapped in the CS NPs by the cross-linking method. The HCT:βCD complex might be mixed with either the CS or the TPP solution during NP preparation, but we decided that it was better to include it in the TPP solution since it did not require heating. The HCT:βCD was added to the TPP phase, and CS NPs containing HCT:βCD were obtained following the conditions used to prepare the control NPs (i.e., NPs without complex). Thus, the presence of HCT:βCD did not substantially alter the features of NPs.

Table 2 summarizes the physicochemical characteristics of CS NPs. Unloaded CS NPs had a particle size of 220 nm, which increased up to 390 nm when HCT:βCD was loaded into the CS NPs. This was due to the inclusion complex being loaded into NPs. The NPs obtained were homogeneous in their size

DOI: 10.1021/acs.molpharmaceut.6b00532
Mol. Pharmaceutics XXXX, XXX, XXX−XXX

and morphology, which was indicated by their PDI values and the SEM study (Table 2 and Figure 1).

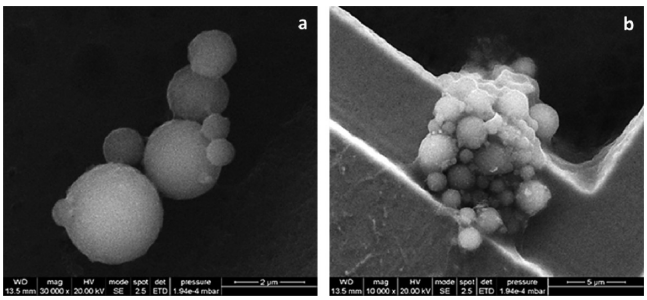

Figure 1. SEM images of CS/HCT:βCD NPs. (a) Scale 2 μm, 30000×. (b) Scale 5 μm, 10000×.

Although, the SEM images showed individual as well as a number of aggregated NPs, they also displayed spherical NPs with a smooth surface. The EDX spectrum of the HCT:βCD-loaded CS NPs is shown in Figure 2.

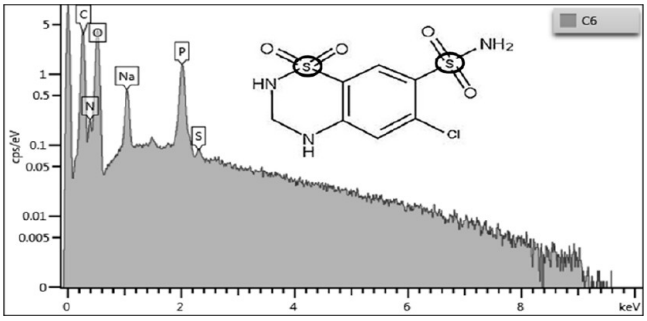

Figure 2. EDX spectrum of CS/HCT:βCD NPs.

A signal corresponding to the elemental S confirmed HCT to be part of the NPs. All unloaded and loaded CS NPs with HCT:βCD exhibited positive ZP values, according to the presence of CS chains (Table 2). The determined encapsulation efficiency (EE) of HCT for CS NPs loaded with HCT:βCD was calculated and was found to be about 0.4 ± 0.1 mg of HCT for each obtained pellet.

3.2. Colloidal Stability of Loaded and Unloaded CS NPs in Aqueous and Buffers Solutions. DLS measurement was applied to investigate the storage stability of CS NPs (empty or loaded with the HCT:βCD inclusion complex) at different pH values and in water solution after 1, 7, 14, and 20 days at room temperature. The results showed that the particles remained relatively stable for at least 20 days in water and buffered solutions, with pH values of 1.2 and 5.5, respectively (Figure 3), with a fast aggregation behavior being observed at pH > 6.8. Moreover, at pH 7.4, the NPs formed aggregates that were too large to be measured by DLS.

This behavior is consistent with the neutralization of the charged $-NH_3^+$ groups in the CS NPs since a high fraction of the amino groups of CS are deprotonated at pH 7.4 (pK_a of CS is about 6.5).[21] This observation is in agreement with previous reports by Brune et al.,[22] who suggested that the colloidal stability of the CS NPs is due to these NPs having a core (a hydrogel) and a shell partway protonated, and therefore, neutralizing the positive charge of the wrapper of the NPs

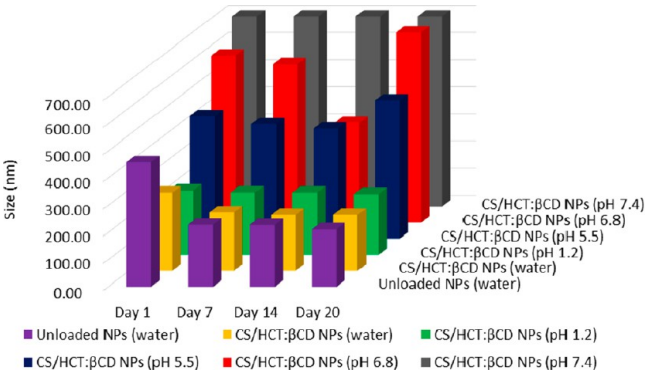

Figure 3. Colloidal stability loaded and unloaded CS NPs with HCT:βCD in aqueous and buffer solutions. Violet, unload NPs; yellow, CS/HCT:βCD NPs (water); green, CS/HCT:βCD NPs (pH 1.2); blue, CS/HCT:βCD NPs (pH 5.5); red, CS/HCT:βCD NPs (pH 6.8); gray, CS/HCT:βCD NPs (pH 7.4).

produces the collapse of the expanded polyelectrolyte chains involved in steric repulsions, yielding a fast aggregation.

3.3. *In Vitro* Release Study. *In vitro* release tests were carried out in order to model the release profiles of HCT from CS/HCT:βCD NPs or the HCT:βCD inclusion complex, in pH conditions similar to that of the GI tract (small intestine). The release of HCT from the CS/HCT:β-CD NPs at different pH values was preliminarily evaluated in the context of the NP stability studies as presented in sections 2.5 and 3.2. As part of those studies, single-point release measurements were performed at each assayed pH value, with it being found that no HCT was released in any case. Consequently, the whole release profile was only determined at pH 7.4, assuming a homologous behavior at other pH values based on the single-point determinations. HCT:βCD-loaded CS NPs did not release quantifiable amounts of HCT at the pH 7.4 studied for 24 h (Figure 4). It is hypothesized that strong interactions

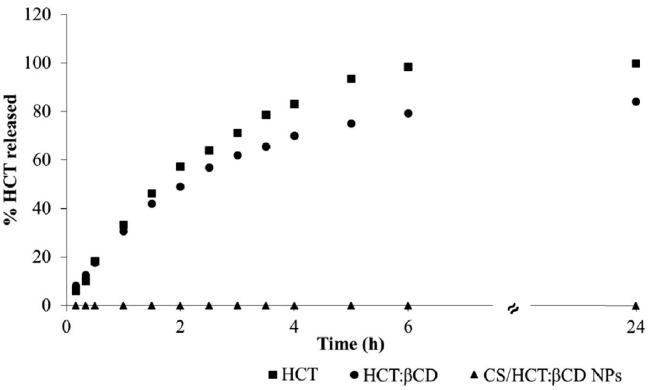

Figure 4. *In vitro* release profiles of HCT, HCT:βCD inclusion complex, and CS/HCT:βCD NPs in phosphate buffer solution at pH 7.4. Red, HCT; green, HCT:βCD; black, CS/HCT:βCD.

between HCT and CS resulted in poor release percentages of HCT from NPs. Moreover, it was observed that NPs retained their morphology and maintained their integrity, which also contributed to the low HCT release.

By comparing the drug release profiles of the free HCT and the HCT:βCD inclusion complex using the f_2 similarity factor,[23] it was found that these drug release profiles were statistically different from each other since a similarity factor

DOI: 10.1021/acs.molpharmaceut.6b00532
Mol. Pharmaceutics XXXX, XXX, XXX−XXX

(f_2) value of 48 was obtained, with the drug release to the receptor medium with the HCT:βCD system being slightly slower than that one obtained with the free drug (Figure 4). This may be attributed to a lower availability of the free drug from its inclusion complex with βCD to cross the semipermeable membrane. These drug release profiles showed an initial burst release (0−6 h), followed by a progressive decrease in the HCT release until reaching a plateau, indicating that complexation of HCT with βCD did not significantly prolong the drug release.

3.4. *In Vitro* Intestinal Mucoadhesion Studies. The *in vitro* association of HCT:βCD-loaded CS NPs (CS/HCT:βCD NPs) with mucin was characterized by measuring the surface charge of CS/HCT:βCD NPs (ZP) under equilibrium conditions before and after mucin addition (Figure 5). The CS/HCT:βCD NPs decreased their surface charge (ΔZP = $ZP_{NPs\text{-}mucin} - ZP_{NPs}$) from +40 to +18 mV (ΔZP of +22) after incubation with mucin.

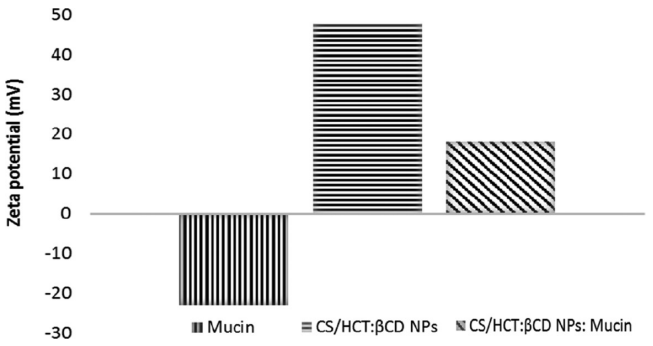

Figure 5. Interactions of CS/HCT:βCD NPs with mucin by dynamic light scattering (DLS).

Mucin has a substantial negative charge, which neutralizes the positive surface charge of NPs formed by CS. The determined ΔZP is an indication that electrostatic interactions occur between NPs and mucin, thus revealing the mucoadhesive potential of these nanosystems.[24] To extend our investigations further, a different approach was used to determine the effect of NPs on the mucin matrix architecture, in the absence or presence of CS/HCT:βCD NPs by SEM. To investigate this, pure mucin and mucin:CS/HCT:βCD NP mixtures were spread out on a slide and air-dried for observation by SEM. Here, the structure of mucin was hydrated to allow the hydrocolloid nature of the highly hydrated mucus covering the mucosal surfaces of the body to be recreated (swollen to ∼95% water). Therefore, samples were prepared without fixation and dehydration, to avoid disturbing the sample in order to observe the mucin gel structure as present in its native network in the mucus.

The structural arrangement of mucin fibers was difficult to observe because of their high hydration state. Figure 6 shows a swollen network formed by mucin fibers, which occupy the total volume of the slide. As can be seen, the microscopic appearance of mucin was modified by the CS/HCT:βCD NPs.

Figure 7 shows that the mucin gel looks dehydrated with a filamentous structure with numerous pores.[25] In addition, NPs with a size of ∼200 nm adhered to the filaments of mucin were also observed. This finding reveals that NPs can bind tightly to mucin, an event that could have an important role in the release mechanism of the encapsulated drug. We concluded that the

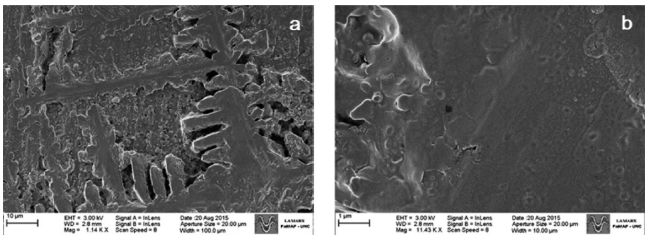

Figure 6. SEM images of PGM. (a) Scale 10 μm, 1140×. (b) Scale 1 μm, 11430×.

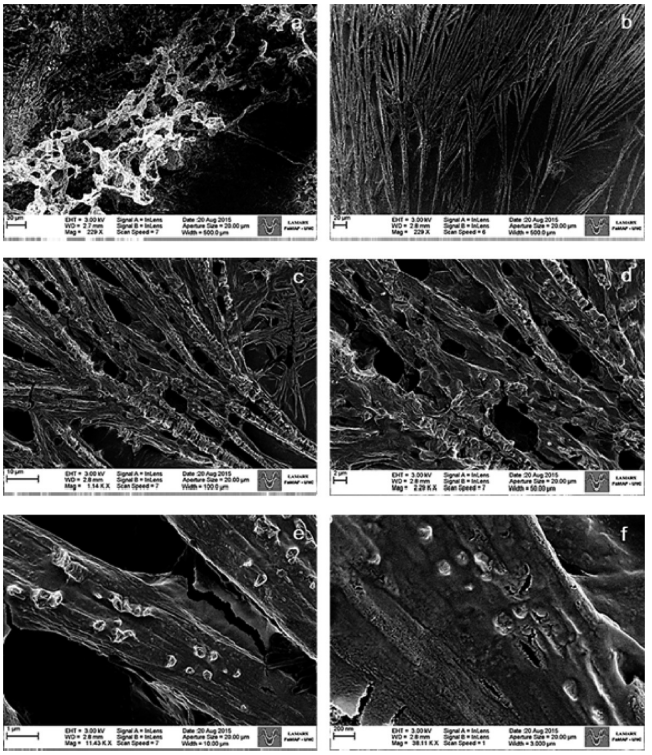

Figure 7. SEM images of PGM incubated with CS/HCT:βCD NPs. (a) Scale 30 μm, 229×. (b) Scale 20 μm, 229×. (c) Scale 10 μm, 1140×. (d) Scale 2 μm, 2290×. (e) Scale 1 μm, 11430×. (f) Scale 200 nm, 38110×.

mucin gel was partially dehydrated and aggregated due to interactions with CS, in agreement with that suggested by Hughes and Marriot, 1984.[26]

3.5. *In Vitro* Intestinal Permeability Studies. The intestinal permeation behavior of the free HCT, HCT:βCD inclusion complex, and HCT CS/HCT:βCD NPs was studied by the gut sac model for 2 h.

A first set of experiments was performed with the aim of assessing the viability and integrity of the intestinal sacs during the experiments with free cultured medium (control), HCT, and CS/HCT:βCD NPs, features that were evaluated by measuring the intestinal sac glucose uptake.

Figure 8 shows that in the presence of CS/HCT:βCD NPs, the glucose content in the serosal side of the sacs remained constant as the incubation time was increased to 120 min, indicating that the intestinal sacs remained viable and functional during the experiments. However, glucose uptake decreased in the presence of free HCT (17 μg/mL) (Figure 8) as time increased to 120 min. This suggests a transporter dysfunction when tissues were exposed to free HCT, which the tissue

DOI: 10.1021/acs.molpharmaceut.6b00532
Mol. Pharmaceutics XXXX, XXX, XXX−XXX

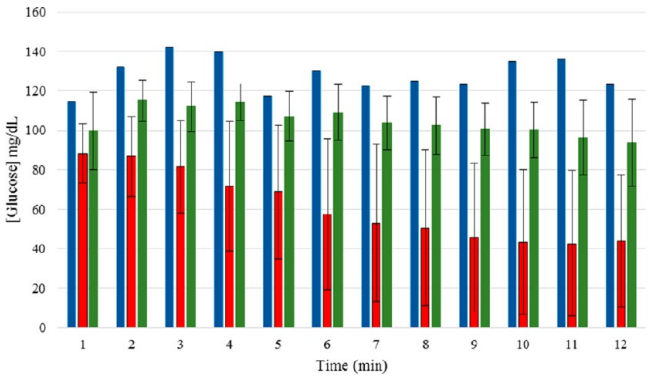

Figure 8. Influence of free HCT and CS/HCT:βCD NPs on the viability of the everted rat gut sacs over the time periods of incubation in the *in vitro* permeability studies. Blue, control; red, HCT; green, CS/HCT:βCD NPs.

dysfunction possibly having occurred due to structural changes in the tissue.

As seen in Figure 9, the absorptive profiles of the free HCT and of the HCT:βCD inclusion complex were not linear, but instead exponential. This effect was observed for the free HCT mucosal solutions containing 750 and 50 μg of HCT (17 and 1 μg/mL, respectively) and for the HCT inclusion complex with βCD, which contained an equivalent amount of HCT of 17 μg/mL. The corresponding flux (F, μg/mL) and apparent permeability coefficients (P_{app}, cm/min) of HCT, at both concentration levels, and of its inclusion complex with βCD, were calculated to obtain the two slopes associated with the exponential permeation profile. The former was between 10 and 60 min, and the latter between 70 and 120 min. Table 3 presents the corresponding values.

It is noteworthy that, the P_{app} values obtained at different concentrations of HCT for the regions of the absorption profiles did not exhibit statistical differences, indicating that the drug permeability was not affected by the drug concentration, which in turn suggested a diffusion controlled permeation mechanism (i.e., there was no transporter involved). A drug permeability behavior for the HCT inclusion complex with βCD similar to that observed with the free HCT was obtained (Figure 9).

It is important to note that the slope change in the absorption profiles of the free drug and its inclusion complex with βCD occurred at the same time (60 min), when the glucose uptake observed in the gut sacs exposed to HCT (Figure 8) started to decrease.

Taking into account that the intestinal tissue exposure to HCT originates a decrease in tissue viability, and possibly in its histological integrity, the exponential permeation pattern of HCT, at both concentrations, or of its inclusion complex with βCD, may be due to this structural tissue damage. In contrast, when the permeation profiles of HCT from the CS/HCT:βCD NPs were determined, it was observed that the amount of HCT in the serosal compartment increased linearly over time (Figure 9), indicating that in the presence of the intestinal tissue, the loaded NPs were able to release HCT, which in turn was available for permeation. Also, the linear permeation pattern observed suggests that the tissue damage observed for the free HCT was not present when the NP carrier system was used.

In order to quantitatively assess the permeability properties of HCT from this system, the F and P_{app} values were calculated. The overall concentration of HCT available for permeation under sink conditions was calculated from the amount of drug present in the mucosal solution (75 $\pm$ 19 μg) at the end of the experiment since this value represents the total amount of HCT liberated from the NP. In this case, the P_{app} value obtained was statistically similar to that obtained from the first portion of the absorption profiles of the free HCT (Table 3). In addition, at the end of the permeation experiments of the CS/HCT:βCD NPs, it was observed that there was a change in the macroscopic appearance of the mucus layer covering the intestinal epithelium of the guts (Figure 10), possibly due to the electrostatic interactions between the CS of the NPs and the mucin present in the mucus layer.[27]

Also, a stability study of CS/HCT:βCD NPs in the culture medium TC199, simulating the experimental conditions of the mucosal side of the rat intestinal sacs, was performed. After

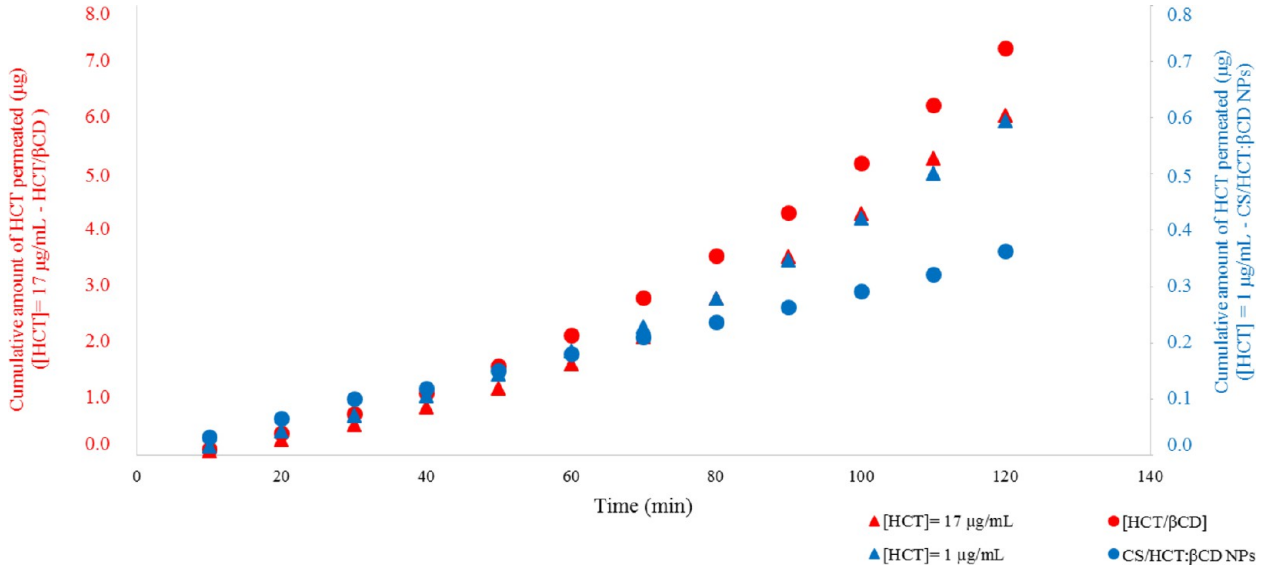

Figure 9. *In vitro* permeability profiles of [HCT] = 17 μg/mL (triangle, red); [HCT] = 1 μg/mL (triangle, blue); HCT:βCD (circle, blue); CS/HCT:βCD (circle, red). Each profile has determined scale that corresponds to a particular color.

DOI: 10.1021/acs.molpharmaceut.6b00532
Mol. Pharmaceutics XXXX, XXX, XXX−XXX

Table 3. Permeability Parameters Following HCT or CS/HCT:βCD NPs Treatments (n = 3)

	time period (min)	HCT (17 μg/mL)	HCT (1 μg/mL)	HCT/βCD (equivalent amount of HCT of 17 μg/mL)	CS/HCT:βCD NPs
flux ± DS (μg/min)	10–60	0.03 ± 0.02	0.003 ± 0.001	0.04 ± 0.01	0.0020 ± 0.0001
	70–120	0.08 ± 0.01	0.007 ± 0.003	0.09 ± 0.01	
P_{app} ± DS (cm/min)	10–60	$(7.5 \pm 2.0) \times 10^{-5}$	$(6.8 \pm 4.4) \times 10^{-5}$	$(9.6 \pm 3.1) \times 10^{-5}$	$(4.9 \pm 1.6) \times 10^{-5}$
	70–120	$(1.9 \pm 0.1) \times 10^{-4}$	$(2.6 \pm 1.1) \times 10^{-4}$	$(2.1 \pm 0.4) \times 10^{-4}$	

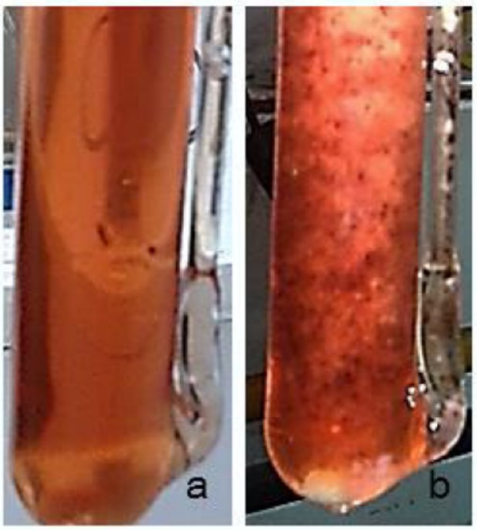

Figure 10. Macroscopic appearance of the mucus layer covering the intestinal epithelium of the gut sacs at the beginning of the experiment (a) and at the end of the permeation assays (b).

incubating CS/HCT:βCD NPs in TC199 medium, phase separation was not observed, but the formation of large aggregates was determined by DLS and showed a similar behavior to that observed with buffer solutions at pH values higher than 6.8.

We attribute the HCT release from the CS/HCT:βCD NPs to mucoadhesive interactions between this system and the mucin present in the mucus layer on the intestinal mucosa. To study further the contribution of mucin triggering the HCT release from NPs, an *in vitro* experiment was performed by incubating CS/HCT:βCD NPs with mucin in a phosphate buffered saline solution at pH 7.4. It was found that free HCT was released to the incubation medium (58 ± 15 μg) in similar quantities to those found with the CS/HCT:βCD NPs in the permeability experiments. These results highlight the role of mucin in controlling the drug release. Similar results were reported by Li et al.,[28] who also obtained a nanosystem described as "mucin-responsive nanoparticles", which was able to provide a controlled release of the loaded drug in the nanosystem in response to mucin.

3.6. Toxicological Evaluation. In order to perform a histopathological and ultrastructural analysis in response to the tissue exposure to HCT under different experimental conditions, cross-sectioned specimens of intestinal sacs exposed to free HCT (17 μg/mL), HCT:βCD (equivalent amount of 17 μg/mL of HCT), or CS/HCT:βCD NPs obtained at the end of the permeation tests were analyzed by high-resolution optical microscopy (LM) and transmission electron microscopy (TEM).

LM and TEM images of the cross-sectioned control samples (unexposed drug gut sacs) are shown in Figure 11.

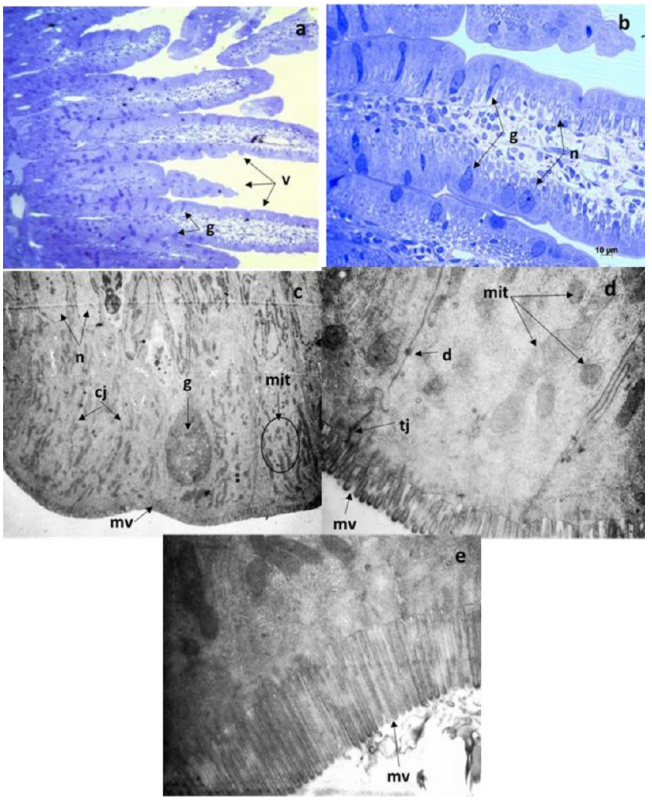

Figure 11. Microphotographs of cross sections of the control intestinal epithelium of rat: (a) 10×, (b) LM 40×, (c) TEM 2156×, (d) TEM 12930×, (e) TEM 16700×. cj, cell junctions; d, desmosomes; g, globet cells; mit, mitochondria; mv, microvilli; n, nuclei; tj, tight junction; v, villus.

LM images revealed no obvious perturbations in villus or crypt organization. The intestinal epithelium appeared normal, with no defects in the enterocyte structure being apparent at this level of resolution. TEM revealed normal cell morphology, with normal nuclei and cellular organelles. The villus was covered with tall columnar absorptive cells presenting long regular and densely packed microvillis. Goblet cells were interspersed among these absorptive cells, with the tight junctions between cells being intact.

We first evaluated whether the gut sacs exposed to the free HCT resulted in any intestinal epithelial injury. Surprisingly, we found unexpected histological changes, such as atrophy of the villus, cell debris, lyses of the intestinal epithelium, and an increase in the number of mononuclear inflammatory cells (Figure 12).

In addition, apoptotic cells were also observed. TEM images showed collagen fibers forming the structure of the connective tissue, an abundant number of vacuoles, and the presence of abundant fenestrated capillaries. These observations are in line with the time-dependent increase in gut permeability of HCT, after the gut sacs were exposed to this drug in the permeability

DOI: 10.1021/acs.molpharmaceut.6b00532
Mol. Pharmaceutics XXXX, XXX, XXX–XXX

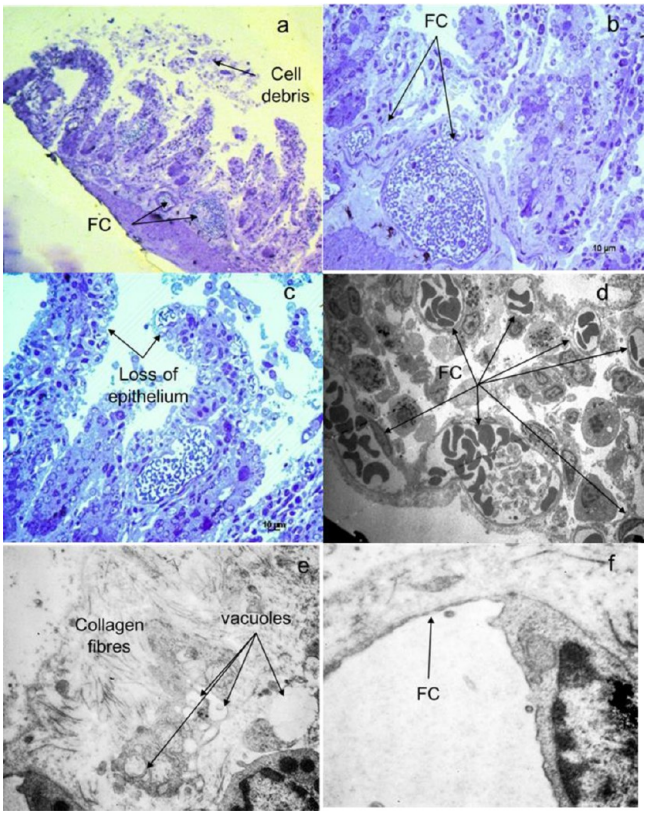

Figure 12. Microphotographs of cross sections of the intestinal epithelium from the gut sac treatment with HCT. (a) LM 10×, (b) LM 40×, (c) LM 40×, (d) TEM 10000×, (f) TEM 16700×. FC, fenestrated capillaries.

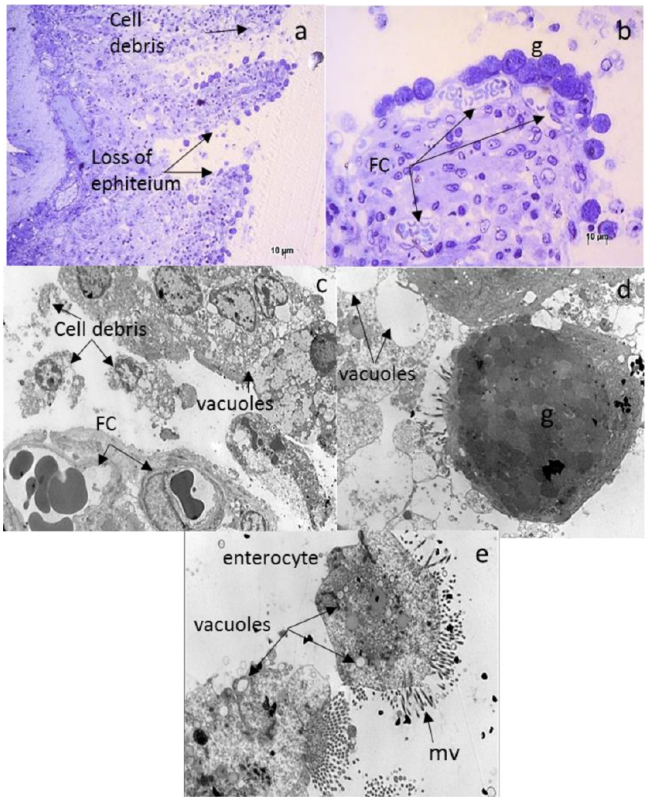

Figure 13. Microphotographs of cross sections of the intestinal epithelium from the gut sac treatment with HCT:βCD. (a) LM 20×, (b) LM 63×, (c) TEM 2156×, (d) TEM 3597×, (e) TEM 4646×. g, globet cells; mv, microvilli; FC, fenestrated capillaries.

assays. To date, no studies have reported these HCT-induced intestinal injuries. However, there are reports on thiazide-induced structural kidney damage.[29,30] A potential mechanism related to HCT-intestinal injury (in addition to other possible mechanisms) may be due to the suppressed enzyme activity of HCT in the Na^+/K^+-ATPase pump on the basolateral side of enterocytes,[31] turning this pump into an open channel conformation that allows sodium influx and potassium efflux. This would lead to a rise in the intracellular concentration of Na^+, which would stimulate the production of superoxide anion and the sustained cellular oxidative stress[32] and trigger a sequence of intracellular cell dysfunction and the impairment of the mitochondrial activity due to an ion imbalance, which is the major cause of mitochondrial damage and subsequent cell death.

Similar structural and ultrastructural microscopic changes in the intestinal epithelium were observed for the rat intestinal sacs treated with the HCT:βCD inclusion complex (Figure 13).

Regarding the gut sacs exposed to CS/HCT:βCD NPs, the histological observations revealed less prominent changes with a better preservation of the intestinal epithelium, showing the presence of an intact gut lumen and villus covered by an epithelial layer (with goblet cells) overlaying the lamina propria, muscularis externa, and serosa (Figure 14).

Nonetheless, some areas exhibited a loss of the intestinal epithelium lining the villus. In addition, we observed desquamated cells in the gut lumen. TEM images showed that the luminal side of enterocytes exhibited some reduction in the microvilli and an increased number of goblet cells in the epithelial layer. Also, on the apical side, intercellular junctions and desmosomes were conserved. The mitochondria were swollen with a severe disorganization of the mitochondrial cristae, and many vacuoles in the cytoplasm were observed. These findings correlate with a decrease in the HCT uptake and a mucus hypersecretion as a protective mechanism, manifested as an increased number of mucus-secreting goblet cells in the mucosa, compared to the free HCT-treated gut sacs during the permeability assays. Also, these cells may be associated with lower intraluminal concentrations of the free drug after the gut sacs were exposed to the CS/HCT:βCD NPs.

We speculate that the lesser degree of injury of HCT in the intestinal mucosa from CS/HCT:βCD NPs may have been due to the slow drug release, thereby acting as a tissue protective delivery vehicle, which prevented the Na^+/K^+-ATPase pump from being exposed to relatively high HCT concentrations, which in turn avoided a dose-dependent inhibition of the Na^+/K^+-ATPase channel.

4. CONCLUSIONS

Our study revealed that the exposure of the intestinal mucosa to free HCT or its inclusion complex with βCD caused greater toxic effects on the intestinal mucosa than those induced by the CS/HCT:βCD NPs-treatment. Furthermore, we obtained different permeability profiles for CS/HCT:βCD NPs compared with free HCT or HCT:βCD inclusion complex, which were linear and exponential, respectively. These data provide new evidence that the oral toxicity of the free HCT or its inclusion complex with βCD is higher than that of the CS/HCT:βCD NPs. We believe that the increased intestinal uptake

DOI: 10.1021/acs.molpharmaceut.6b00532
Mol. Pharmaceutics XXXX, XXX, XXX−XXX

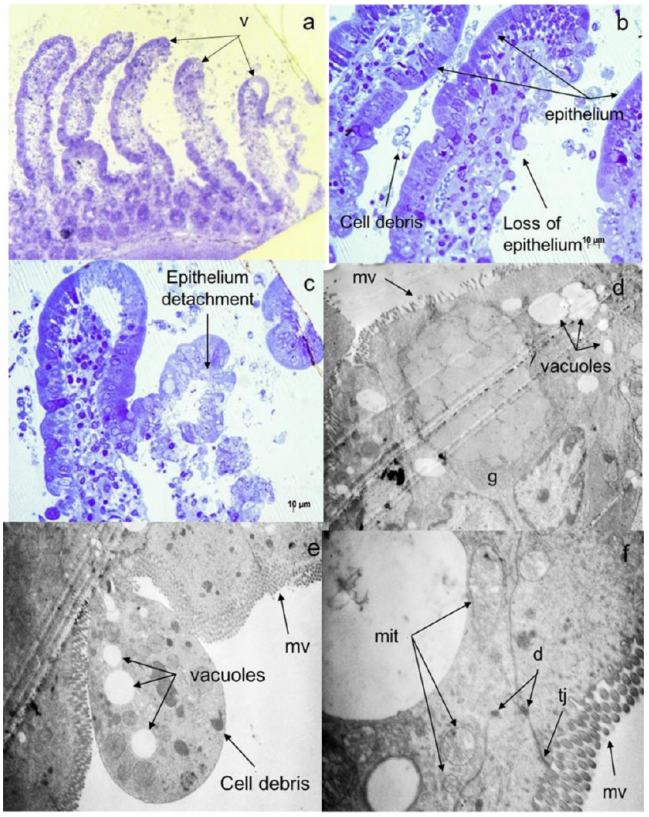

Figure 14. Microphotographs of cross sections of the intestinal epithelium from the gut sac treatment with CS/HCT:βCD NPs. (a) LM 10×, (b) LM 40×, (c) LM 40×, (d) TEM 4646×, (e) TEM 4646×, (f) TEM 12939×. d, desmosomes; g, globet cells; mit, mitochondria; mv, microvilli; tj, tight junction; v, villus.

and severe tissue injury of HCT in the intestinal epithelium could be directly related to possible effects of this drug on the ionoregulatory Na^+/K^+-ATPase channel. Furthermore, based on mucoadhesion studies, it is postulated that CS/HCT:βCD NPs may increase the gastrointestinal retention of the HCT, probably attributed to electrostatic interactions, which provide increased adherence to the mucus barrier lining the intestinal epithelium that promoted the HCT release from the NPs. Thus, this system acts as an efficient delivery vehicle for the modulated release of HCT, which in turn maintains a lower and sustained drug concentration within the gut lumen when compared to the administration of free HCT and the HCT:βCD inclusion complex. This feature would lead to less severe local tissue injury.

AUTHOR INFORMATION

Corresponding Author

*E-mail: glagra@fcq.un.edu.ar. Tel: 54-351-5353865.

Notes

The authors declare no competing financial interest.

ACKNOWLEDGMENTS

We thank FONCyT (Préstamo BID 1728/OC-AR, PICT 1376), the Secretaría de Ciencia y Técnica de la Universidad Nacional de Córdoba (SECyT), and the Consejo Nacional de Investigaciones Científicas y Tecnológicas de la Nación (CONICET) for their financial support.

REFERENCES

(1) Messerli, F. H.; Bangalore, S. Half a century of hydrochlorothiazide: facts, fads, fiction, and follies. *Am. J. Med.* **2011**, *124*, 896−899.
(2) Sica, D. A.; Carter, B.; Cushman, W.; Hamm, L. Thiazide and loop diuretics. *J. Clin. Hypertens.* **2011**, *13*, 639−643.
(3) Ono, A.; Sugano, K. Application of the BCS biowaiver approach to assessing bioequivalence of orally disintegrating tablets with immediate release formulations. *Eur. J. Pharm. Sci.* **2014**, *64*, 37−43.
(4) El-Gizawy, S. A.; Osman, M. A.; Arafa, M. F.; EL Maghraby, G. M. Aerosil as a novel co-crystal co-former for improving the dissolution rate of hydrochlorothiazide. *Int. J. Pharm.* **2015**, *478*, 773−778.
(5) Singh, R.; Lillard, J. W. Nanoparticle-based targeted drug delivery. *Exp. Mol. Pathol.* **2009**, *86*, 215−223.
(6) Swierczewska, M.; Han, H. S.; Kim, K.; Park, J. H.; Lee, S. Polysaccharide-based naoparticles for theranostic nanomedicine. *Adv. Drug Delivery Rev.* **2016**, *99*, 70−84.
(7) Bugnicourt, L.; Alcouffe, P.; Ladaviere, C. Elaboration of chitosan nanoparticles: favorable impact of a mild thermal treatment to obtain finely divided, spherical, and colloidally stable objects. *Colloids Surf., A* **2014**, *457*, 476−486.
(8) Kaloti, M.; Bohidar, H. B. Kinetics of coacervation transition versus nanoparticle formation in chitosan-sodium tripolyphosphate solutions. *Colloids Surf., B* **2010**, *81*, 165−173.
(9) Wang, J. J.; Zeng Xiao, R. Z.; Zhou, G. L.; Zhan, X.; Wang, S. L. Recent advances of chitosan nanoparticles as drug carriers. *Int. J. Nanomed.* **2011**, 765−774.
(10) Jingou, J.; Shilei, H.; Weiqi, L.; Danjun, W.; Tengfei, W.; Yi, X. Preparation, characterization of hydrophilic and hydrophobic drug in combine loaded chitosan/cyclodextrin nanoparticles and *in vitro* release study. *Colloids Surf., B* **2011**, *83*, 103−107.
(11) Valente, A. J. M.; Carvalho, R. A.; Söderman, O. Do cyclodextrins aggregate in water? Insights from NMR experiments. *Langmuir* **2015**, *31*, 6314−6320.
(12) Onnainty, R.; Schenfeld, E. M.; Quevedo, M. A.; Fernández, M. A.; Longhi, M. R.; Granero, G. E. Characterization of the hydrochlorothiazide:β-cyclodextrin inclusioncomplex. *J. Phys. Chem. B* **2013**, *117*, 206−217.
(13) Trapani, A.; Lopedota, A.; Franco, M.; Cioffi, N.; Ieva, E.; García-Fuentes, M.; Alonso, M. J. A comparative study of chitosan and chitosan/cyclodextrin nanoparicles as potential carriers for the oral delivery of small peptides. *Eur. J. Pharm. Biopharm.* **2010**, *75*, 26−32.
(14) Fan, W.; Yan, W.; Xu, Z.; Ni, H. Formation mechanism of monodisperse, low molecular weight chitosan nanoparticles by ionic gelation technique. *Colloids Surf., B* **2012**, *90*, 21−27.
(15) Takeuchi, H.; Thongborisute, J.; Matsui, Y.; Sugihara, H.; Yamamoto, H.; Kawashima, Y. Novel mucoadhesion tests for polymers and polymer-coated particles to design optimal mucoadhesive drug delivery systems. *Adv. Drug Delivery Rev.* **2005**, *57*, 1583−1594.
(16) Lifschitz, A.; Virkel, G.; Ballent, M.; Sallovitz, J.; Lanusse, C. Combined use of ivermectin and triclabendazole in sheep: in vitro and in vivo characterization of their pharmacological interaction. *Vet. J.* **2009**, *182*, 261−268.
(17) Sharma, P.; Chawla, H. P. S.; Panchagnula, R. LC determination of cephalosporins in vitro rat intestinal sac absorption model. *J. Pharm. Biomed. Anal.* **2002**, *27*, 39−50.
(18) Quevedo, M. A.; Briñón, M. C. In vitro and in vivo pharmacokinetic characterization of two novel prodrugs of zidovudine. *Antiviral Res.* **2009**, *83*, 103−111.
(19) Quevedo, M. A.; Nieto, L. E.; Briñón, M. C. P-glycoprotein limits the absorption of the anti-HIV drug zidovudine through rat intestinal segments. *Eur. J. Pharm. Sci.* **2011**, *43*, 151−159.
(20) Rampino, A.; Borgogna, M.; Blasi, P.; Bellich, B.; Cesaro, A. Chitosan nanoparticles: Preparation, size evolution and stability. *Int. J. Pharm.* **2013**, *455*, 219−228.
(21) Shan, D.; Han, E.; Xue, H. G.; Cosnier, S. Self-assembled films of hemoglobin/lapanite/chitosan: Application for the direct electro-

DOI: 10.1021/acs.molpharmaceut.6b00532
Mol. Pharmaceutics XXXX, XXX, XXX−XXX

chemistry and catalysis to hydrogen peroxide. *Biomacromolecules* **2007**, *8*, 3041−3046.
(22) Brunel, F.; Véron, L.; Ladaviere, C.; David, L.; Domard, A.; Delair, T. Synthesis and structural characterization of chitosan nanogels. *Langmuir* **2009**, *25*, 8935−8943.
(23) FDA. *FDA Guidance for Industry: Immediate Release Solid Dosage Forms: Scale-up and Post Approval Changes (SUPAC-IR). Chemistry, manufacturing and controls: In vitro dissolution testing and in vivo bioequivalence documentation*; Food and Drug Administration: Rockville, MD, 1995.
(24) Sogias, I. A.; Williams, A. C.; Khutoryanskiy, V. V. Why is chitosan mucoadhesive? *Biomacromolecules* **2008**, *9*, 1837−1842.
(25) Znamenskaya, Y.; Sotres, J.; Engblom, J.; Arnebrant, T.; Kocherbitov, V. Effect of hydratation on structural and thermodynamic properties of pig gastric and bovine submaxillary glan mucins. *J. Phys. Chem. B* **2012**, *116*, 5047−5055.
(26) Crowther, R. S.; Hughes, D. R. L.; Marriot, C. Mucus glycoprotein gels: A scanning electron microscopy study of the effect of cations. *Micron Microsc. Acta* **1984**, *15*, 37−45.
(27) Nordgård, C. T.; Nonstand, U.; Olderoy, M.; Espevik, T.; Draget, K. I. Alterations in mucus barrier function and matrix structure induced by guluronate oligomers. *Biomacromolecules* **2014**, *15*, 2294−2300.
(28) Li, C.; Liu, Z.; Yan, X.; Lu, W.; Liu, Y. Mucin-controlled drug release from mucoadhesive phenylboronic acid-rich nanoparticles. *Int. J. Pharm.* **2015**, *479*, 261−264.
(29) Reungjui, S.; Hu, H.; Mu, W.; Roncal, C. A.; Croker, B. P.; Patel, J. M.; Nakagawa, T.; Srinivas, T.; Byer, K.; Simoni, J.; Wesson, D.; Sitprija, V.; Johnson, R. J. Thiazide-induced subtle renal injury not observed in states of equivalent hypokalemia. *Kidney Int.* **2007**, *72*, 1483−1492.
(30) Ellison, D. H.; Loffing, J. Thiazide effects and adverse effects: insights from molecular genetics. *Hypertension* **2009**, *54*, 196−202.
(31) Saha, P.; Manoharan, P.; Arthur, S.; Sundaram, S.; Kekuda, R.; Sundaram, U. Molecular mechanism of regulation of villus cel Na-K-ATPase in the chronically inflamed mammalian small intestine. *Biochim. Biophys. Acta, Biomembr.* **2015**, *1848*, 702−711.
(32) Yu, S. P. Na^+, K^+-ATPase: the new face of an old player in pathogenesis andapoptotic/hybrid cell death. *Biochem. Pharmacol.* **2003**, *66*, 1601−1609.

DOI: 10.1021/acs.molpharmaceut.6b00532
Mol. Pharmaceutics XXXX, XXX, XXX−XXX